Single-Sample Finger Vein Recognition via Competitive and Progressive Sparse Representation

Pengyang Zhao, Zhiquan Chen, Jing-Hao Xue, *Senior Member, IEEE,* Jianjiang Feng, *Member, IEEE,* Wenming Yang, *Senior Member, IEEE,* Qingmin Liao, *Senior Member, IEEE,* and Jie Zhou, *Senior Member, IEEE*

Abstract—As an emerging biometric technology, finger vein recognition has attracted much attention in recent years. However, single-sample recognition is a practical and longstanding challenge in this field, referring to only one finger vein image per class in the training set. In single-sample finger vein recognition, the illumination variations under low contrast and the lack of information of intra-class variations severely affect the recognition performance. Despite of its high robustness against noise and illumination variations, sparse representation has rarely been explored for single-sample finger vein recognition. Therefore, in this paper, we focus on developing a new approach called Progressive Sparse Representation Classification (PSRC) to address the challenging issue of single-sample finger vein recognition. Firstly, as residual may become too large under the scenario of single-sample finger vein recognition, we propose a progressive strategy for representation refinement of SRC. Secondly, to adaptively optimize progressions, a progressive index called Max Energy Residual Index (MERI) is defined as the guidance. Furthermore, we extend PSRC to bimodal biometrics and propose a Competitive PSRC (C-PSRC) fusion approach. The C-PSRC creates more discriminative fused sample and fusion dictionary by comparing residual errors of different modalities. By comparing with several state-of-the-art methods on three finger vein benchmarks, the superiority of the proposed PSRC and C-PSRC is clearly demonstrated.

Index Terms—Finger vein, finger dorsal texture, progressive sparse representation, competitive sparse fusion

1 Introduction

In this paper, we focus on a challenging practical topic: developing a robust approach to finger vein recognition under the single training sample per class.

In recent years, hand-based biometrics become more and more popular due to their high user acceptance, low device requirement, and superior performance [1]–[4]. As one of the important hand-based biometrics, finger vein trait refers to the networks of blood vessels beneath the finger skin. The characteristics of liveness detection and difficulty for forgery of finger vein recognition have interested many researchers. For example, Repeated Line Tacking (RLT) [5] extracted binary finger vein patterns by using the characteristic that the pixel intensity of background is higher than that of vein areas in finger vein images. Miura et al. [6] developed the Local Maximum Curvature (LMC) of the cross-section profile to improve the robustness of binary finger vein patterns. The discriminative orientation features of the finger vein were extracted via a bank of Gabor filters [7]. Yang et al. [8] proposed a binary direction coding method to encode the vein pattern containing directional information. A new bit-consistent structure of binary features by considering sparse constraints is proposed in [9]. Further, Yang et al. [10] used low-rank representation for robust finger vein recognition. To make features more robust and discriminative, some researchers introduced minutiae-based methods into finger vein recognition. Meng et al. [11] extracted refined finger vein minutia features by adopting a zone-based minutia matching technique. Considering both the orientation and curvature information, the anatomy structure and imaging characteristics of vein patterns is fully explored in [12]. A novel framework was proposed in [13] to improve both accuracy and efficiency, which incorporated an indexing method and a matching method. Prommegger et al. [1] gave a systematic study about the interference of finger rotation and proposed two angle correction approaches to deal with it. With the blossom of deep learning, some researchers introduced deep learning into finger vein recognition. For example, Hou et al. [14] combined convolutional autoencoder and Support Vector Machine (SVM) to apply finger vein recognition. FV-GAN was proposed in [15] by employing Generative Adversarial Networks (GAN) to extract binary vein patterns for recognition. By replacing Euclidean distance with cosine distance, Hou et al. [16] proposed a new loss function named ArcVein for finger vein recognition.

However, two great challenges still remains in the area of finger vein recognition: low quality imagery and single training sample per class.

Illumination variations under low contrast are common in finger vein images, resulting in some blurred and noisy regions (see Fig. 1). Once the regions of interest (ROI) in finger vein images are noisy and ambiguous, many methods [6], [11], [12] may produce unreliable features, and ulti-

Pengyang Zhao, Zhiquan Chen, Wenming Yang and Qingmin Liao are with Shenzhen International Graduate School / Department of Electronic Engineering, Tsinghua University, China. (Corresponding author: Wenming Yang, yangelwm@163.com.)
Jing-Hao Xue is with the Department of Statistical Science, University College London, UK.
Jianjiang Feng and Jie Zhou are with the Department of Automation, Tsinghua University, China.
Manuscript received April 19, 2005; revised August 26, 2015.

mately their recognition performance is compromised. Fortunately, it was revealed that SRC is robust against illumination variations and corruption [17], [18]. There have been several SRC-based methods for finger vein recognition [19]–[21]. Specifically, Xin et al. [19] employed conventional SRC on finger vein recognition for the first time. Shazeeda et al. [20] proposed Mutual SRC and a new decision rule to improve the performance of conventional SRC on finger vein recognition. Recently, a Weighted SRC (WSRC) method was developed in [21].

However, in the single-sample protocol, these SRC-based methods show unsatisfactory results. The reason is that there is only limited information of intra-class variations, and the irrelevant training samples pose severe disturbances on the recognition under this circumstance. Therefore, in this paper we focus on addressing this issue and propose a new SRC-based model for single-sample finger vein recognition. Specifically, to alleviate the interference of those training samples deviating from the test one, we progressively eliminate the dictionary atoms whose sparse coefficients are smaller than a threshold by iteratively applying the sparse representation on the test sample. To adapt to different test images, we design a new index named Max Energy Residual Index (MERI) to guide our algorithm to stop at an appropriate time, obtaining a more compact dictionary and a more representative spare vector for recognition.

In summary, this paper makes four main contributions:

1) We propose a Progressive Sparse Representation Classification (PSRC) approach to tackling single-sample finger vein recognition. We design a progressive strategy of sparse representation by progressively removing the dictionary atoms deviating from the test sample to reconstruct a more compact and less redundant dictionary. With this dictionary, a more representative sparse vector is obtained for recognition.
2) To guide the progression of PSRC, we propose a new index called MERI to obtain adaptive progressions of different samples. MERI considers both max entry energy and residual error, resulting in better recognition performance and reasonable time consumption.
3) We extend PSRC to finger-based bimodal biometric recognition, named Competitive Progressive Sparse Representation Classification (C-PSRC) algorithm. C-PSRC embeds PSRC into a competitive strategy and exploits the competitive strength of two modalities. Integrating the progressive approach and the competitive strategy, C-PSRC is capable of constructing more discriminative fused sample and fusion dictionary.
4) The proposed methods are compared with many state-of-the-art algorithms on three public databases. Extensive experimental results demonstrate the effectiveness and superiority of our PSRC and C-PSRC on unimodal finger vein recognition and bimodal recognition under the single-sample protocol, respectively.

The rest of this paper is organized as follows. Section 2 reviews several topics related to our work. Section 3 describes the motivation and details of proposed PSRC and its bimodal extension C-PSRC is presented in Section 4. Section 6 evaluates the proposed methods on three widely used databases. Conclusions are drawn in Section 7.

2 Related Work

2.1 SRC

With sufficient data, a sample $\boldsymbol{y}$ can be represented as a sparse linear combination with respect to other samples from the same class [22]:

$$\boldsymbol{y} = \boldsymbol{V}\boldsymbol{x_0} + \boldsymbol{z}, \tag{1}$$

where $\boldsymbol{y} \in \mathbb{R}^d$ is the test sample; matrix $\boldsymbol{V} = [\boldsymbol{V_1}, \boldsymbol{V_2}, \ldots, \boldsymbol{V_k}] \in \mathbb{R}^{d\times n}$ denotes the training set with k classes; for the n_i samples from the ith class, we denote them as a submatrix $\boldsymbol{V_i} \in \mathbb{R}^{d\times n_i}$; $\boldsymbol{x_0} \in \mathbb{R}^n$ is a sparse vector whose entries are ideally zero except for those associated with class i if $\boldsymbol{y}$ belongs to that class; and $\boldsymbol{z} \in \mathbb{R}^d$ is a noise term. The theory of compressed sensing reveals that, if the solution of $\boldsymbol{x_0}$ is sparse enough, it can be recovered efficiently by solving an ℓ_1-minimization problem [23]:

$$\widehat{\boldsymbol{x}}_{\boldsymbol{1}} = \arg\min \|\boldsymbol{x}\|_1,\ s.t.\ \|\boldsymbol{V}\boldsymbol{x} - \boldsymbol{y}\|_2 \le \varepsilon. \tag{2}$$

The classification criterion of SRC is that given the sparse vector $\widehat{\boldsymbol{x}}_{\boldsymbol{1}}$, $\delta_i(\widehat{\boldsymbol{x}}_{\boldsymbol{1}})$ is a new vector whose nonzero terms are the ones that in $\widehat{\boldsymbol{x}}_{\boldsymbol{1}}$ associated with class i. Only using items associated with class i, the test sample $\boldsymbol{y}$ can be approximated as $\widehat{\boldsymbol{y}}_{\boldsymbol{i}} = \boldsymbol{V}\delta_i(\widehat{\boldsymbol{x}}_{\boldsymbol{1}})$. Then $\boldsymbol{y}$ would be classified by minimizing the residual r_i between $\boldsymbol{y}$ and $\widehat{\boldsymbol{y}}_{\boldsymbol{i}}$ [24]:

$$\arg\min_i\ r_i(\boldsymbol{y}) = \|\boldsymbol{y} - \boldsymbol{V}\delta_i(\widehat{\boldsymbol{x}}_{\boldsymbol{1}})\|_2. \tag{3}$$

Based on the above theory, SRC and its variants have achieved impressive success in face recognition [17], [25]–[29]. For example, Wright et al. [17] revealed that the choice of feature space is no longer critical if the test sample can be approximated by a sparse linear combination of training samples. Both registration and illumination variations were considered during sparse representation [25]. For under-sampled or occlusion scenario, Deng et al. [26] constructed the dictionary with training samples and intra-class variants to get satisfactory performance. A two-phase SRC-based method was proposed in [27]. In [28], a new dictionary was constructed by class centroids and the sample-to-centroid distance, while in [29] the dictionary was constructed by patches of random positions. Different from the above work, we construct the dictionary by progressively eliminating the irrelevant atoms, resulting in a more compact dictionary for robust single-sample finger vein recognition.

2.2 Biometric recognition under single-sample protocol

Biometric recognition under the single-sample protocol is a practical and challenging problem. Limited information of intra-class variations and severe disturbances from similar classes deteriorate the algorithm performance, making the single-sample problem even harder. A variety of methods are proposed to tackle this issue [30]–[33]. For instance, Yang et al. [30] tackled the single-sample finger vein recognition by encoded brightness differences in the finger vein image to obtain finger vein patterns, which contain the orientation information of veins. Sparse Variation Dictionary Learning (SVDL) [31] learned a compact variation dictionary which incorporates various variations to handle the single-sample face recognition problem. Chan et al. [32] proposed a deep

model named PCANet, which consisted two stages by learning multiple filter banks with PCA for single-sample face recognition and image classification. Recently, Fei et al. [33] proposed a hashing learning method named Learning Compact Multifeature Codes (LCMFC). LCFMC exploits multifeatures of the palmprint and learns a compact hash code for single-sample palmprint recognition. In our work, we adopt the sparse representation for the first time to tackle single-sample finger vein recognition and progressively discard the training samples deviating from the test one since they pose undesirable disturbances on the recognition results.

3 Progressive Sparse Representation Classification

In this section, we first detail the motivation and procedure of our proposed method PSRC. Then we give an explanation of PSRC from a probabilistic perspective.

3.1 PSRC

As aforementioned, most SRC-based methods perform well under dense-sample circumstances but poorly in single-sample environments. The reason is that once the number of training samples per subject is only one, the interference from similar samples makes nonzero entries in $\widehat{\boldsymbol{x}}_{\mathbf{1}}$ not concentrate on the correct position. In finger vein images, there are some differences between test and training images due to the illumination variations under low contrast. For example, Fig. 1 shows some raw finger vein images, from which we can observe that illumination variations overwhelm the real finger vein points in some regions. In this case, the samples from other subjects would pose more interference to the sparse representation of the test image. As a result, the residual $\|\boldsymbol{V}\boldsymbol{x}-\boldsymbol{y}\|_2$ in Eq. 2 may become too large, which makes the sparse vector $\widehat{\boldsymbol{x}}_{\mathbf{1}}$ no longer play a decisive role in the classification. Hence it is more likely to get a better classification if we can construct a new compact dictionary which contain fewer interfering atoms. This intuition inspires us to propose a new SRC-based method to progressively discard atoms to construct more compact, less redundant dictionaries adaptively for different test samples. We name our method PSRC. Specifically, in PSRC, the atoms deviating from the test one are discarded progressively since they do not contribute much to the classification of the test sample. By "progressively" we mean that our method consists of a number of iterations, and the dictionary atoms with coefficients smaller than a predefined threshold λ_{th} would be discarded iteration by iteration.

Moreover, the classification criterion of conventional SRC is unsuitable for the single-sample problem because the residual of one training sample cannot represent the residual of the entire subject. Hence, in order to adapt to the single-sample scenario, an alternative classification rule is adopted for PSRC: the label associated with the largest entry in the sparse vector is assigned to the test image.

Now, a remaining problem to be tackled is when to stop progressions of PSRC. In general, a small residual indicates a good sparse representation, and the energy is retained by the corresponding dictionary atoms [17]. Inspired by that, we propose a new index MERI as the guidance, represented

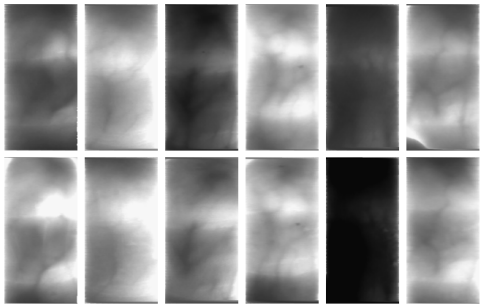

Fig. 1. Paired raw finger vein images from six fingers. Images in the upper row are training images and in the lower row are test images.

by μ, to adaptively control the iterations of PSRC. MERI is a weighted sum of two terms, defined as follows:

$$\mu = \beta\frac{\max(\widehat{\boldsymbol{x}}_{\mathbf{1}})}{\|\widehat{\boldsymbol{x}}_{\mathbf{1}}\|_2^2} + (1-\beta)\frac{\|\boldsymbol{y}-\boldsymbol{V}\widehat{\boldsymbol{x}}_{\mathbf{1}}\|_2^2}{\|\boldsymbol{y}\|_2^2}W, \tag{4}$$

where $\frac{\max(\widehat{\boldsymbol{x}}_{\mathbf{1}})}{\|\widehat{\boldsymbol{x}}_{\mathbf{1}}\|_2}$ is the proportion of the largest entry in the sparse vector $\widehat{\boldsymbol{x}}_{\mathbf{1}}$, which we call Max Energy Index (MEI); $\frac{\|\boldsymbol{y}-\boldsymbol{V}\widehat{\boldsymbol{x}}_{\mathbf{1}}\|_2^2}{\|\boldsymbol{y}\|_2^2}$ is the standardized residual of test image $\boldsymbol{y}$; the hyper-parameter β controls the trade-off between MEI and the standardized residual; and W is the parameter to ensure the MEI and the residual have the same order of magnitude.

In the single-sample protocol, the test sample is classified according to the largest coefficient in the sparse vector. In this sense, two terms in Eq. 4 have clear meanings. If the first term (i.e., MEI term) is sufficiently large, the result would be more persuasive. The incorrect result is more likely to occur if the second term, standardized residual, is too large. With the guidance of MERI, PSRC can be stopped automatically, leading to a sparse vector with a sufficiently large entry and a reasonable residual. Fig. 2 shows the variations of MEI and the residual with the iterations of PSRC on THU-FVFDT2 database. It shows that MEI increases faster than standardized residual as PSRC proceeds. We summarize the procedure of PSRC in Algorithm 1.

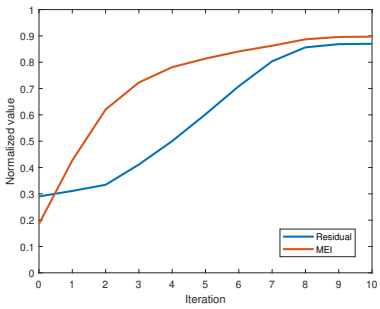

Fig. 2. The MEI and the residual after each iteration of PSRC.

3.2 An explanation of PSRC

Generally speaking, classification could be modeled as a maximum posterior probability problem. Let $\boldsymbol{y}$ denote the test sample and c represent the label of $\boldsymbol{y}$:

$$\hat{c} = \arg\max_{c} \; P(c|\boldsymbol{y}). \tag{5}$$

Algorithm 1 Progressive Sparse Representation Classification (PSRC)

Input: A matrix of training samples $\boldsymbol{V} = [\boldsymbol{V}_1, \boldsymbol{V}_2, \ldots, \boldsymbol{V}_k] \in \mathbb{R}^{d\times k}$, one sample for each of the k classes, where $\boldsymbol{V}_i \in \mathbb{R}^d$, $i \in \{1, \ldots, k\}$, is a column vector. A test sample $\boldsymbol{y} \in \mathbb{R}^d$. Parameter β, MERI threshold μ_{th} and coefficient threshold λ_{th}.

Output: The class label of the test sample $\boldsymbol{y}$.

1: Calculate sparse representation of $\boldsymbol{y}$ via Eq. 2.
2: Compute MERI with the sparse vector via Eq. 4.
3: Discard the atoms with coefficients smaller than λ_{th}.
4: If MERI $< \mu_{th}$, **repeat** 1, 2, 3; else, **go to** 5.
5: Assign the class label associated with the largest entry of the sparse vector to the test sample $\boldsymbol{y}$.

After applying the sparse representation of test sample $\boldsymbol{y}$, $\boldsymbol{y}$ could be represented by the sparse vector $\boldsymbol{\alpha}$:

$$\hat{c} = \arg\max_{c} \; P(c|\boldsymbol{\alpha}). \tag{6}$$

In the single-sample problem, the test image is classified into the class with the largest coefficient [34]. In other words, the test sample should not belong to the class with a smaller coefficient in the single-sample problem. The probability that a test sample belongs to the ith class is related to the ith coefficient if it is greater than a threshold λ_{th}, i.e.,

$$P(c = i|\boldsymbol{\alpha}) \begin{cases} \propto \alpha_i, & \text{if } \alpha_i > \lambda_{th}; \\ = 0, & \text{if } \alpha_i \leq \lambda_{th}, \end{cases} \tag{7}$$

where α_i represents the coefficient corresponding to the training sample in the ith class. With a threshold λ_{th}, we can normalize the probability in Eq. 7 as

$$P(c = i|\boldsymbol{\alpha}) = \begin{cases} \frac{\alpha_i}{\sum_{\alpha_j > \lambda_{th}} \alpha_j}, & \text{if } \alpha_i > \lambda_{th}; \\ 0, & \text{if } \alpha_i \leq \lambda_{th}. \end{cases} \tag{8}$$

The dictionary is updated with the progression of PSRC. Most discarded training samples (i.e., dictionary atoms) have lower similarity to the test image according to Eq. 8. Since the training samples with lower similarity have been discarded, the maximum of $P(c|\boldsymbol{\alpha})$ would be expected to increase with updating, as shown in Fig. 3.

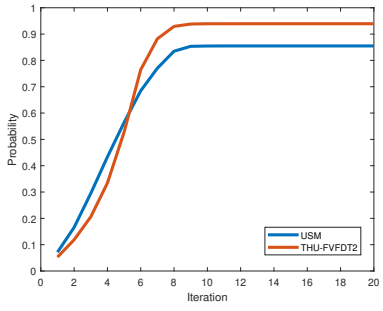

Fig. 3. Average probability of classifying $\boldsymbol{y}$ into the class corresponding to the largest coefficient in $\boldsymbol{\alpha}$. USM [35] and THU-FVFDT2 [36] are two public finger vein databases.

Furthermore, as shown in Fig. 4, the maximum probability (calculating via Eq. 8) of most test samples is no more than 0.2 after the first iteration of PSRC. The maximum probability distributing in a narrow range with small value gives an unreliable result. After the last iteration of PSRC, more samples can be classified with much stronger confidence as the distribution of the maximum probability is much closer to 1. As a result, PSRC achieves remarkable enhancement through discarding the training samples that deviate from the test one.

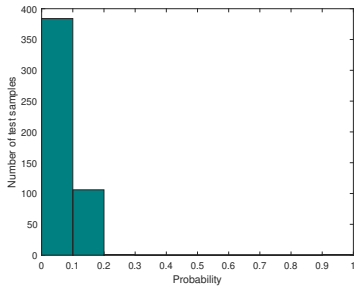

(a)

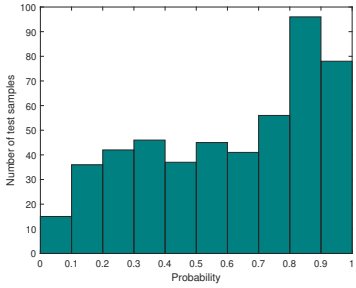

(b)

Fig. 4. (a) Largest probability distribution after the first iteration of PSRC. (b) Largest probability distribution after the last iteration of PSRC.

4 Competitive PSRC: An Extension of PSRC to Bimodality

To further explore the potential of bimodal PSRC for enhancing single-sample finger vein recognition, we propose C-PSRC by fusing finger vein and finger dorsal texture images.

In the corresponding images, finger veins are mainly distributed vertically while finger dorsal textures are distributed horizontally. So finger vein and finger dorsal texture are naturally complementary in terms of their directional information. In addition, there is strong spatial correlation between the two modalities as they were captured simultaneously for the same finger. A more discriminative sample could be acquired when complementary information and spatial correlation are preserved during the fusion process. Therefore, a two-stage competitive fusion model called C-PSRC is proposed with the first stage for fusion and the second stage for reconstruction of fused dictionaries based on PSRC, which combines finger vein and finger dorsal texture features. The diagram of C-PSRC is shown in Fig. 5, and the procedure is summarized in Algorithm 2.

C-PSRC aims to enhance the discriminability between different subjects by using the pixel-level fusion in finger vein and finger dorsal texture images of the same subjects. In the first stage of C-PSRC, the finger vein and finger dorsal

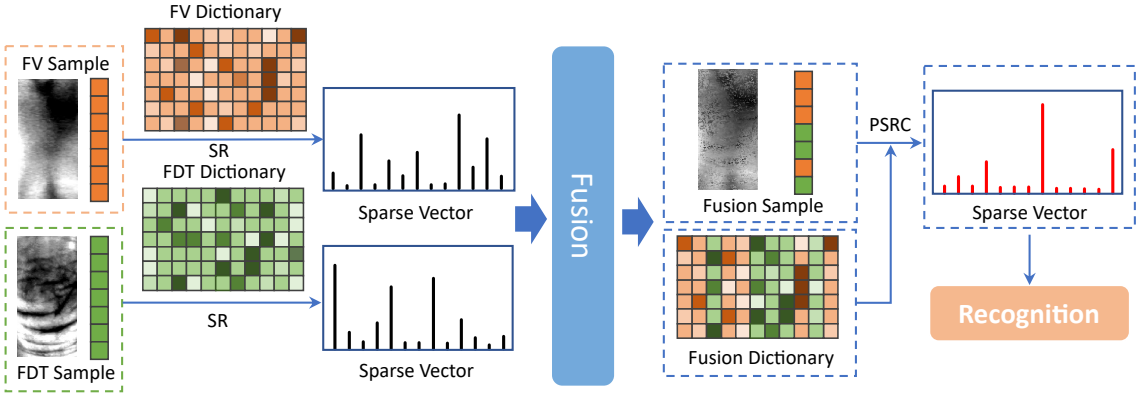

Fig. 5. The diagram of proposed competitive sparse fusion (C-PSRC).

Algorithm 2 Competitive Progressive Sparse Representation Classification (C-PSRC)

Input: A matrix of FV training samples $\boldsymbol{X}^{\mathrm{fv}} = [\boldsymbol{X}_1^{\mathrm{fv}}, \boldsymbol{X}_2^{\mathrm{fv}}, \ldots, \boldsymbol{X}_k^{\mathrm{fv}}] \in \mathbb{R}^{d\times k}$. A matrix of finger dorsal texture training samples $\boldsymbol{X}^{\mathrm{fdt}} = [\boldsymbol{X}_1^{\mathrm{fdt}}, \boldsymbol{X}_2^{\mathrm{fdt}}, \ldots, \boldsymbol{X}_k^{\mathrm{fdt}}] \in \mathbb{R}^{d\times k}$. A test FV sample $\boldsymbol{y}^{\mathrm{fv}} \in \mathbb{R}^d$ and a test finger dorsal texture sample $\boldsymbol{y}^{\mathrm{fdt}} \in \mathbb{R}^d$ from the same subject.

Output: The class label of the test sample $\boldsymbol{y}^{\mathrm{fv}}$ and $\boldsymbol{y}^{\mathrm{fdt}}$.

1: Calculate sparse vectors of $\boldsymbol{y}^{\mathrm{fv}}$ and $\boldsymbol{y}^{\mathrm{fdt}}$ based on $\boldsymbol{X}^{\mathrm{fv}}$ and $\boldsymbol{X}^{\mathrm{fdt}}$, respectively.
2: Compute the reconstruction error of $\boldsymbol{y}^{\mathrm{fv}}$ and $\boldsymbol{y}^{\mathrm{fdt}}$ via Eq. 9 and Eq. 10.
3: Construct the fused sample $\boldsymbol{y}^{\mathrm{F}}$ and the dictionary $\boldsymbol{D}^{\mathrm{F}}$ via Eq. 11 and Eq. 12.
4: Implement PSRC to the fused sample $\boldsymbol{y}^{\mathrm{F}}$ based on the fused dictionary $\boldsymbol{D}^{\mathrm{F}}$ via Algorithm 1.

texture images are fused under the SRC framework. The reconstruction error of each modality is adopted to measure the discriminability of each pixel in test images. For the ith pixel in the finger vein test sample $\boldsymbol{y}^{\mathrm{fv}}$, the reconstruction error r_i^{fv} is defined as

$$r_i^{\mathrm{fv}} = |y_i^{\mathrm{fv}} - \boldsymbol{V}_i^{\mathrm{fv}}\boldsymbol{X}^{\mathrm{fv}}|, \tag{9}$$

where y_i^{fv} is the ith pixel value in the finger vein test sample; $\boldsymbol{V}_i^{\mathrm{fv}}$ denotes the ith row of the finger vein dictionary; and $\boldsymbol{X}^{\mathrm{fv}}$ represents the sparse vector from Eq. 2. Analogously, the reconstruction error of the ith pixel in the finger dorsal texture sample $\boldsymbol{y}^{\mathrm{fdt}}$ is defined as

$$r_i^{\mathrm{fdt}} = |y_i^{\mathrm{fdt}} - \boldsymbol{V}_i^{\mathrm{fdt}}\boldsymbol{X}^{\mathrm{fdt}}|, \tag{10}$$

where the notations are the same as in Eq. 9, but for finger dorsal texture now. Then the fused sample $\boldsymbol{y}^F$ can be obtained by

$$y_i^F = \begin{cases} y_i^{\mathrm{fv}} & r_i^{\mathrm{fv}} < r_i^{\mathrm{fdt}}; \\ y_i^{\mathrm{fdt}} & r_i^{\mathrm{fv}} \geq r_i^{\mathrm{fdt}}. \end{cases} \tag{11}$$

A new dictionary $\boldsymbol{D}^F$ can then be derived as

$$\boldsymbol{D}_i^F = \begin{cases} \boldsymbol{V}_i^{\mathrm{fv}} & r_i^{\mathrm{fv}} < r_i^{\mathrm{fdt}}; \\ \boldsymbol{V}_i^{\mathrm{fdt}} & r_i^{\mathrm{fv}} \geq r_i^{\mathrm{fdt}}, \end{cases} \tag{12}$$

where $\boldsymbol{D}_i^F$ denotes the ith row of the fused dictionary $\boldsymbol{D}^F$.

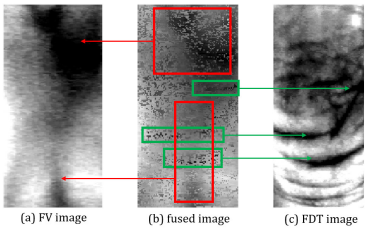

Fig. 6. The fused test image. Red rectangles indicate finger vein regions and green rectangles indicate finger dorsal texture regions.

The motivation of the fusion strategy is that if the reconstruction error of a test finger vein image pixel is smaller than the counterpart of finger dorsal texture, the pixel in the finger vein image is more discriminative. Therefore, pixels in finger vein and finger dorsal texture images compete for the corresponding pixel position in the fused image. An example of a fusion result is shown in Fig. 6. It is evident that the fused image contains rich texture information from both finger vein and finger dorsal texture. Instead of a universal dictionary, a new dictionary associated with the fused test image is constructed. Therefore, the superiority of fused test image is guaranteed and the performance of the proposed method is boosted.

Once the fused sample $\boldsymbol{y}^{\mathrm{F}}$ and the associated dictionary $\boldsymbol{D}^{\mathrm{F}}$ are obtained, PSRC is performed with respect to $\boldsymbol{y}^{\mathrm{F}}$ and $\boldsymbol{D}^{\mathrm{F}}$ for recognition.

5 Discussion

The difference between few-shot learning (FSL) techniques and our PSRC is discussed in this section.

As one of the most often used meta-learning benchmarks [37], [38], FSL aims to give the model the ability to fast adapt to new tasks [39], labels [40], or categories [41], [42] with little training data. It is motivated by the humanity's fast adaption to new knowledge based on experience [43]. Due to the lack of target task data, recent FSL models learn from separate large, labeled task-disjoint or class-disjoint base sets initially, and then adapt to new tasks or classes with a few samples in the support set and the query set for evaluation [38], [42].

Fundamentally different from FSL methods, the label sets of our test set and training set overlap. We aim to label

a probe sample with seen labels in the gallery, rather than a new unseen label. In addition, PSRC does not need to acquire any meta knowledge or train on a separate large, labeled finger vein database as the base set in advance. PSRC progressively discards atoms in the training set to construct more compact, less redundant dictionaries adaptively for different probe samples, thus obtaining accurate results.

6 Experimental Analysis

In this section, we conduct extensive experiments to evaluate the effectiveness of our proposed method PSRC from different perspectives. Three public finger vein databases are adopted, including the THU-FVFDT2 [36], USM [35] and SDUMLA databases [44]. In addition, various finger vein recognition approaches are performed, including classical traditional methods and deep learning-based methods. In our experiments, deep learning-based methods are implemented using the PyTorch framework, and trained on an Nvidia GTX 1080Ti GPU. Traditional methods are implemented with Matlab2019b on a PC with Core(TM)i5-4590 CPU 3.30 GHz and 8.00 GB RAM in a 64-bit Windows 10 operating system.

6.1 Databases

The THU-FVFDT2 database [36] contains 610×4 finger vein and finger dorsal texture images extracted from 610 different fingers (two finger vein images and two finger dorsal texture images per subject). The majority of the subjects are students and staff volunteers from college. The ROI is provided with a size of 200×100.

The USM database [35] is captured from the index and middle fingers on both hands of 123 volunteers, resulting in a total of 492 classes. For each finger, 12 images were collected. In addition, the ROI is provided with a size of 300×100.

The SDUMLA database [44] is captured from the index, middle, and ring fingers on both hands of 106 volunteers. Totally, there are 3,816 finger vein images in this database. Each class has six samples.

In our experiments, the ROIs of SDUMLA are first extracted according to [30] and then all ROIs are resized into 200×100.

To simulate the single-sample protocol, we randomly select one sample per class in the first session of each database as the training image, and the images captured in the second session are taken as the test images.

6.2 Evaluation details

We apply each algorithm to two tasks, namely finger vein identification and finger vein verification, to thoroughly assess their performance on single-sample finger vein recognition.

Finger vein identification is a 1 vs. N matching process to determine the tester's identity registered in the database. Accuracy (ACC) [45] is calculated to evaluate identification performance as

$$\mathrm{ACC} = \frac{\text{Number of correctly classified samples}}{\text{Total number of samples}}. \quad (13)$$

Finger vein verification is a typical 1 vs. 1 matching process to determine whether each matching is a "genuine matching" or an "imposter matching". A "genuine matching" means that two matching samples are from the same finger, and otherwise the matching is named as "imposter matching". Equal Error Rate (EER) [45] is used as the metric, which is the point where the False Accept Rate (FAR) and the False Reject Rate (FRR) are the same. FAR and FRR are calculated as

$$\mathrm{FAR} = \frac{\text{Number of false acceptance}}{\text{Number of total matching}}, \quad (14)$$

$$\mathrm{FRR} = \frac{\text{Number of false rejection}}{\text{Number of total matching}}. \quad (15)$$

Additionally, we also report the FRR value by fixing FAR at a specific value x, denoted as FRR@FAR = x.

6.3 Ablation studies of PSRC

6.3.1 PSRC versus SRC

In this subsection, experiments are conducted to study the difference between SRC and PSRC, and prove that SRC is not suitable for single-sample problem, but PSRC works well in this situation.

Given a new test finger vein sample, we computed its sparse representation based on SRC and PSRC, respectively. Fig. 7 shows coefficients in two calculated sparse vectors. For convenience, the two Y-axes in Fig. 7 have the same range. Obviously, the vector of PSRC is more sparse than that of SRC with the same length. More entries corresponding to lower correlation classes are equal to zero, which indicates that the training samples preserved by PSRC are more representative. It is easier for PSRC to find that the test sample should be classified into the 9th class in Fig. 7(b), which obviously has the largest entry in the sparse vector.

6.3.2 Effectiveness of MERI

In this subsection, we conduct experiments to verify the effectiveness of the progression index MERI. MERI considers both MEI and the residual in a joint manner, which enables PSRC to stop progressions adaptively for different samples. As a baseline, we apply PSRC without the guidance of MERI, but with a fixed number of iterations. Table 1 shows the results in terms of ACC and EER. We can see that, for this baseline, an increase of the number of iterations does not lead to better performance. This phenomenon is due to that fixing the same iteration number for all samples in PSRC may lead to redundant dictionaries or unideal sparse vectors. In contrast, MERI allows PSRC to exit at an appropriate time, which depends on the test sample itself and the threshold μ_{th}. Hence, PSRC could generate a more compact dictionary and obtain a more representative sparse vector for recognition with the guidance of MERI, which assigns an adaptive number of iterations to different test samples rather than using a fixed one.

6.4 Comparison of PSRC with State-of-the-art

6.4.1 Finger vein verification

To evaluate the effectiveness of the proposed PSRC, we compare PSRC with some classical and state-of-the-art finger

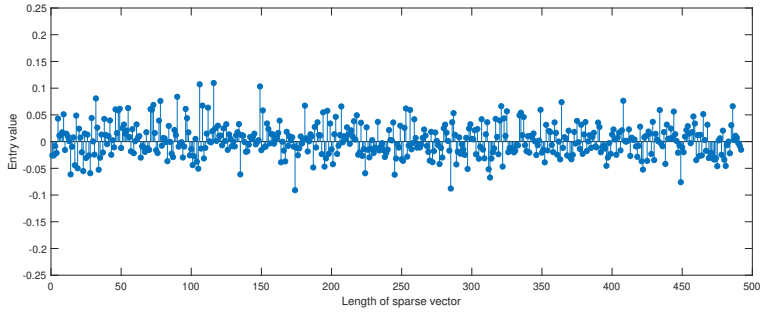

(a)

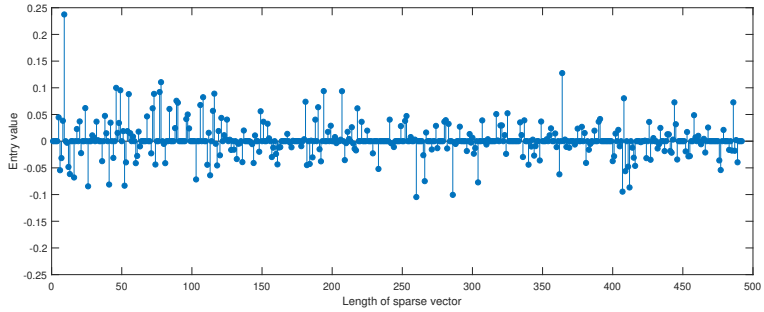

(b)

Fig. 7. Sparse vectors calculated by SRC and PSRC on a test image from the USM database. (a) The sparse vector calculated by SRC. (b) The sparse vector calculated by PSRC.

TABLE 1
Performance of the PSRC with the guidance of MERI and the PSRC with a fixed number of iterations

#Iterations of PSRC	ACC (%)	EER (%)
1	90.04	4.61
2	90.85	3.80
3	92.48	3.05
4	94.31	2.86
5	93.90	3.07
with MERI	**94.51**	**2.55**

vein verification algorithms, including SRC-based methods, vein pattern-based methods and deep learning-based methods. The results on the three databases are listed in Table 2, Table 3, and Table 4, respectively.

From the results, we can make the following observations. Firstly, extracting finger vein patterns using LMC [6] and Location Direction Coding (LDC) [30] produce poor EER on all databases. Secondly, the insightful approach RLT [5] and FV-GAN [15] perform excellently on THU-FVFDT2 but poorly on USM and SDUMLA. In our experiment, the FVGAN does not converge on the SDUMLA database, and its results are not included in the tables. Thirdly, MRFBCNN [46] outperforms other CNN-based methods, indicating the importance of higher-order statistics in the feature extraction of finger veins. Fourthly, the performance of the CNN-based methods [14]–[16], [47] is sometimes not as good as traditional methods. One reason is that, even with the data augmentation, the capacity of CNNs is limited by insufficient training data, especially in the single-sample protocol. Additionally, overfitting easily occurs with limited samples, which also degrades the performance. Fifthly, compared with SRC-based methods (i.e., SRC [17], WSRC [21], and KCDVD [48]), the results indicate that our PSRC exhibits competitive performance. It demonstrates that PSRC has a strong ability to handle the single-sample problem. In short, from the results listed in Table 2, 3, 4, PSRC performs the best on both THU-FVFDT2 and USM, and ranks second on SDUMLA.

The superior performance of PSRC can be attributed to at least two factors: 1) By discarding some dictionary atoms that may disturb correct classification, PSRC produces a compact dictionary for each test sample, significantly improving the performance. 2) With the support of the iterative index MERI, PSRC can stop progressions adaptively for different samples. In that case, PSRC can find a more compact and less redundant dictionary than other SRC-based methods.

TABLE 2
Verification performance (%) of different methods on the THU-FVFDT2 database.

Method	EER (%)	FRR@FAR=1%	FRR@FAR=0.1%
RLT [5]	1.72	2.30	7.87
LMC [6]	4.16	6.89	15.74
LDC [30]	2.12	2.79	6.56
PWBDC [49]	1.64	2.62	12.79
Hong et al. [47]	1.96	2.95	12.46
Hou et al. [14]	1.15	1.24	9.67
FV-GAN [15]	2.38	2.95	7.54
MRFBCNN [46]	0.60	0.33	2.79
ArcVein [16]	3.27	8.03	20.83
SRC [17]	1.15	1.35	4.59
KCDVD [48]	6.03	10.00	20.98
WSRC [21]	0.83	0.66	3.77
PSRC	**0.41**	**0**	**2.46**

TABLE 3
Verification performance (%) of different methods on the USM database.

Method	EER (%)	FRR@FAR=1%	FRR@FAR=0.1%
RLT [5]	6.46	9.55	14.43
LMC [6]	7.34	8.74	14.99
LDC [30]	5.73	12.13	24.26
PWBDC [49]	4.79	8.74	13.82
Hong et al. [47]	6.50	13.62	22.15
Hou et al. [14]	6.26	12.40	22.97
FV-GAN [15]	7.48	10.57	13.82
MRFBCNN [46]	3.66	5.28	11.99
ArcVein [16]	6.09	8.94	14.13
SRC [17]	4.61	6.50	11.18
KCDVD [48]	9.57	17.07	28.86
WSRC [21]	5.74	8.13	**10.98**
PSRC	**2.55**	**2.85**	12.92

TABLE 4
Verification performance (%) of different methods on the SDUMLA database.

Method	EER (%)	FRR@FAR=1%	FRR@FAR=0.1%
RLT [5]	11.29	15.72	17.92
LMC [6]	5.03	6.29	7.08
LDC [30]	6.74	9.43	13.36
PWBDC [49]	6.60	12.42	20.77
Hong et al. [47]	4.99	9.91	16.67
Hou et al. [14]	7.39	14.31	23.90
MRFBCNN [46]	3.71	6.29	14.15
ArcVein [16]	4.32	10.38	22.64
SRC [17]	4.86	7.08	10.53
KCDVD [48]	8.01	13.99	20.75
WSRC [21]	**2.44**	8.94	16.83
PSRC	3.61	**4.56**	**6.29**

6.4.2 *Finger vein identification*

In the identification protocol, the test finger vein image should be assigned a label by comparing it to training images. We report the results on the three databases in Table 5. Since the mode collapse occurs on the SDUMLA database, we omit the result of FVGAN on the SDUMLA database. From the result, we can observe that PSRC consistently obtains satisfactory performance. The accuracy of PSRC on the THU-FVFDT2 and USM is the highest, which are 97.05% and 94.51%, respectively. It is worth noting that the PSRC ranks third on the SDUMLA database, which is still a competitive result compared to other methods.

TABLE 5
ACC (%) on the THU-FVFDT2, USM and SDUMLA databases.

Methods	THU-FVFDT2	USM	SDUMLA
RLT [5]	96.72	86.79	83.49
LMC [6]	87.54	88.82	93.08
LDC [30]	95.25	87.05	88.37
PWDBC [50]	96.87	90.85	84.28
Hong et al. [47]	95.08	78.66	90.41
Hou et al. [14]	93.28	78.86	75.47
FV-GAN [15]	95.57	89.23	-
MRFBCNN [46]	83.16	86.59	78.77
ArcVein [16]	**98.85**	89.02	86.01
SRC [17]	95.98	90.04	87.97
KCDVD [48]	74.10	68.70	72.48
WSRC [21]	96.23	89.43	**94.74**
PSRC	97.05	**94.51**	92.70

6.5 Parameter analysis

In this subsection, we conduct a series experiments to find optimal settings for the parameters.

As above mentioned, there are three tuning parameters (β, μ_{th} and λ_{th}) in PSRC. Firstly, we set β as an arithmetic progression in $[0, 1]$ with a common difference 0.1 and μ_{th} in $[1, 3]$ with a common difference 0.2. Fig. 8 illustrates variations of EER with different combinations of β and μ_{th} on three databases. From the results, one can see that β and μ_{th} with larger value can obtain better and stabler results on USM and SDUMLA. On THU-FVFDT2, PSCR achieves the best verification performance when $\beta = 0.7$ and $\mu_{th} \in [2.2, 2.4]$. What is more, for all three databases, better performance can be obtained with a larger β, which means that the MEI term plays a vital role during the iterations of PSRC.

Then, we experiment λ_{th} in $[-0.5, 0.5]$ with a step of 0.1 and fix $\beta = 0.7, \mu_{th} = 2.2$ to study the effect of λ_{th}. The results are shown in Fig. 9. From the results, an observation is that PSRC obtains the best verification performance when $\lambda_{th} = 0$ on the three databases. In addition, performance degradation occurs when λ_{th} is too large.

Based on the above experiments, we set $\beta = 0.7$, $\mu_{th} = 2.2$ and $\lambda_{th} = 0$ in this paper.

6.6 Analysis of Failure Cases

To fully investigate PSRC, we analysed some failure cases from the THU-FVFDT2 database (shown in Fig. 10) and summarized two types of samples that PSRC found challenging. The limitations of our approach were then discussed.

1) Samples with big intraclass variations. Since the intraclass variations are inaccessible under the single-sample scenario, such samples are difficult to handle. When training samples and test samples have big differences, PSRC fails to obtain a correct prediction. In addition, in this situation, the sparse vectors also indicate that PSRC struggles to assign the sample to the correct category since more non-zeros items with large values are retained in this case. Some samples are shown in Fig. 10(a) and Fig. 10(b).

2) Samples with little valid finger vein information. Different samples may have similar background variations or intensity distributions. In the case of little valid finger vein information, background cues dominate the representation process in PSRC. In this case, PSRC tends to assign the sample to a wrong category with similar background cues. This case is shown in Fig. 10(c).

After analysing the failure cases, we can identify some limitations of PSRC. PSRC struggles to handle some hard samples like the two types mentioned above. The coefficients for the correct categories are highlighted in the red rectangle in the fourth column of Fig. 10. We can observe that the coefficient of the correct category is comparatively large, but not the largest. This indicates that PSRC can retain the desired dictionary atoms but may fail to obtain correct predictions in those two cases.

6.7 Running time analysis of PSRC

In this subsection, the running time of our PSRC and other finger vein recognition methods are compared. The feature extraction time and feature matching time of each method on the THU-FVFDT2 and USM databases are calculated and reported in Table 6. As can be seen from Table 6, our PSRC achieves the fastest feature matching process. Since PSRC contains multiple iterations, it costs more time on feature

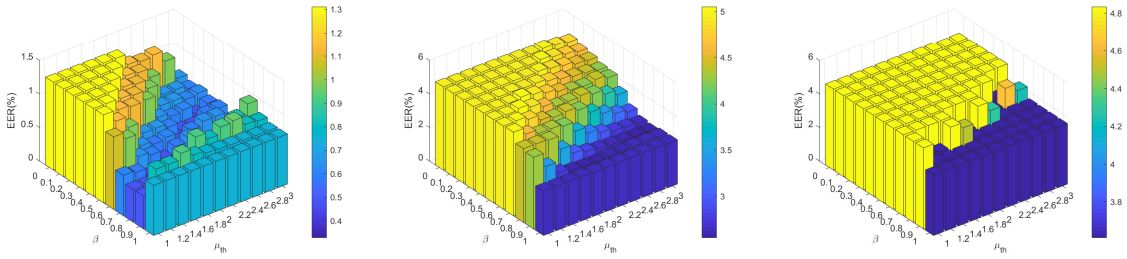

(a) (b) (c)

Fig. 8. Variations of EER (%) versus parameters of β and μ_{th} on (a) THU-FVFDT2, (b) USM, (c) SDUMLA, respectively.

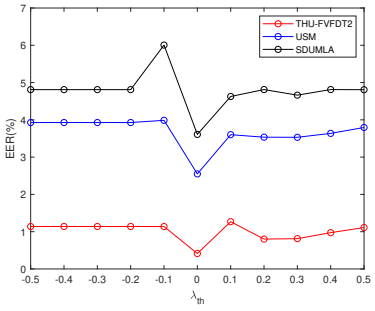

Fig. 9. Variations of EER (%) versus λ_{th} on three databases.

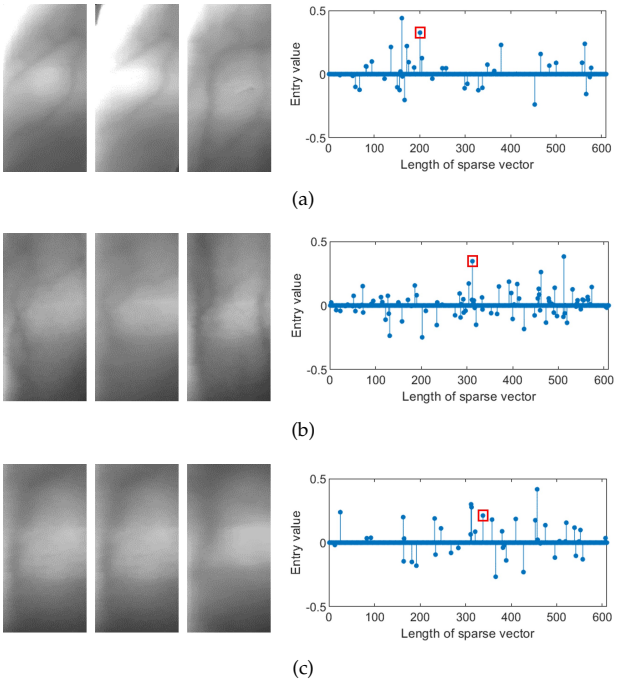

(a) (b) (c)

Fig. 10. Some failure cases of PSRC. Each row represents a failure case. For each case, the first column is the test sample, the second column is the correct gallery sample, the third column is the gallery sample from the assigned category, and the fourth column is the sparse vector produced by PSRC. We highlight the correct coefficient in the sparse vector by a red rectangle.

extraction than other SRC-based methods except for WSRC, which spends a lot of time calculating the weights.

TABLE 6
Running time (seconds) on the THU-FVFDT2 and USM databases of different methods.

Methods	THU-FVFDT2		USM	
	Feature Extraction	Matching	Feature Extraction	Matching
RLT [5]	2.3246	0.1621	2.5751	0.2133
LMC [6]	0.2390	0.1063	0.2220	0.1301
LDC [30]	0.1277	0.2162	0.1171	0.2465
PWBDC [49]	**0.0789**	0.0580	**0.0887**	0.0432
SRC [17]	0.8462	0.0246	1.0153	0.0289
KCDVD [48]	0.7123	2.2790	0.5417	2.3440
WSRC [21]	3.3435	0.0303	3.0119	0.0295
PSRC	1.4130	**0.0231**	1.8934	**0.0257**

6.8 Effectiveness of C-PSRC

In Section 4, we give the extension model of PSRC for bimodal biometrics, named C-PSRC. In this subsection, the effectiveness of C-PSRC is evaluated by two sets of experiments from unimodal and bimodal perspectives, respectively.

Firstly, experiments are designed to compare the effectiveness of C-PSRC with various classical unimodal algorithms. The experimental results are listed in Table 2 and Table 7. We depict the detection error tradeoff (DET) curves in Fig. 11 and Fig. 12. The DET curve is a plot of FAR and FRR. As can be seen from the unimodal results, C-PSRC significantly outperforms the unimodal methods in terms of EER. Such a good performance could be ascribed to two factors: 1) Finger vein and finger dorsal texture provide complementary information and spatial correlation. C-PSRC effectively combines and obtains more valid information. 2) For each fused test image, a new fused dictionary is constructed with better representation and discrimination ability. The fused test images along with the new dictionary contribute to the improvement of the performance.

TABLE 7
Comparison C-PSRC with unimodal methods on finger dorsal texture.

Method	LMC	RLT	LDC	LLBP	Hong et al.	C-PSRC
EER(%)	2.61	6.48	0.92	1.75	2.68	**0.16**
ACC(%)	92.46	83.11	97.54	95.90	90.25	**99.02**

Secondly, in order to prove the effectiveness of C-PSRC strictly, extensive experiments are conducted to compare C-PSRC with other bimodal methods. Table 8 shows the

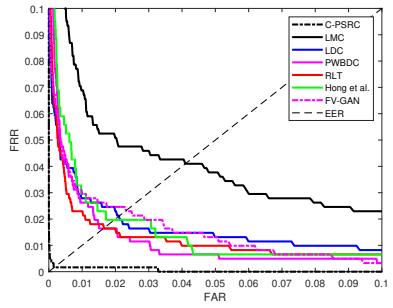

Fig. 11. DET plot of C-PSRC and different algorithms on finger vein trait.

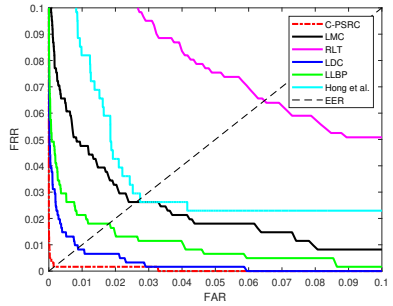

Fig. 12. DET plot of C-PSRC and different algorithms on finger dorsal texture.

experimental results and Fig. 13 illustrates the DET curves of these algorithms. Compared with the unimodal results, almost all the bimodal models obtain better performance, proving the superiority of exploiting complementary information from finger vein and finger dorsal texture. This indicates that the fusion of finger vein and finger dorsal texture is a promising direction for improving finger-based recognition. Moreover, the comparison results also reveal that C-PSRC performs the best among the bimodal algorithms, demonstrating the effectiveness of our C-PSRC.

TABLE 8
Comparison C-PSRC with various bimodal approaches.

Method	Zhang et al. [51]	C^2Code [52]	LLBP	C-PSRC
EER(%)	1.27	0.43	0.71	**0.16**
ACC(%)	98.20	**99.02**	98.85	**99.02**

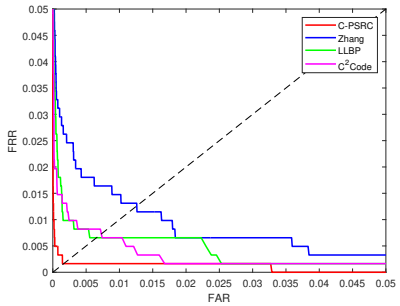

Fig. 13. DET plot of different bimodal methods.

7 Conclusion

In this paper, we propose PSRC for single-sample finger vein recognition. By discarding the atoms deviating from the test sample progressively, PSRC endows test samples with more compact dictionaries for better representation. In addition, an index named MERI is defined to guide the PSRC to perform adaptive progressions for different test samples. Experimental results show that our PSRC remarkably outperforms other classical and state-of-the-art methods.

Furthermore, we extend PSRC to bimodal biometrics for single-sample finger vein and finger dorsal texture recognition. C-PSRC embeds a competitive selection mechanism into PSRC for single-sample finger vein and finger dorsal texture recognition. Compared with other unimodal and bimodal methods, C-PSRC achieves the lowest EER and the highest accuracy.

As a successful attempt, PSRC and C-PSRC provide two new and promising perspectives for single-sample finger vein recognition.

Acknowledgment

This work was partly supported by the Natural Science Foundation of China (No. 62171251), the Natural Science Foundation of Guangdong Province (No. 2020A1515010711) and the Special Foundation for the Development of Strategic Emerging Industries of Shenzhen (Nos. JCYJ20170817161845824 and JCYJ20200109143035495).

References

[1] B. Prommegger, C. Kauba, M. Linortner, A. Uhl, Longitudinal finger rotation—deformation detection and correction, IEEE Transactions on Biometrics, Behavior, and Identity Science 1 (2) (2019) 123–138.
[2] L. Fei, B. Zhang, Y. Xu, D. Huang, W. Jia, J. Wen, Local discriminant direction binary pattern for palmprint representation and recognition, IEEE Transactions on Circuits and Systems for Video Technology 30 (2) (2019) 468–481.
[3] Y. Xu, G. Lu, Y. Lu, F. Liu, D. Zhang, Fingerprint pore comparison using local features and spatial relations, IEEE Transactions on Circuits and Systems for Video Technology 29 (10) (2018) 2927–2940.
[4] S. Li, B. Zhang, Joint discriminative sparse coding for robust hand-based multimodal recognition, IEEE Transactions on Information Forensics and Security 16 (2021) 3186–3198.
[5] N. Miura, A. Nagasaka, T. Miyatake, Feature extraction of finger-vein patterns based on repeated line tracking and its application to personal identification, Machine Vision and Applications 15 (4) (2004) 194–203.
[6] N. Miura, A. Nagasaka, T. Miyatake, Extraction of finger-vein patterns using maximum curvature points in image profiles, IEICE Transactions on Information and Systems 90 (8) (2007) 1185–1194.
[7] A. Kumar, Y. Zhou, Human identification using finger images, IEEE Transactions on Image Processing 21 (4) (2012) 2228–2244.
[8] W. Yang, W. Ji, F. Zhou, Q. Liao, Robust hybrid finger pattern identification using intersection enhanced Gabor based direction coding, IEICE Transactions on Information and Systems 99 (10) (2016) 2668–2671.
[9] H. Liu, G. Yang, L. Yang, Y. Yin, Learning personalized binary codes for finger vein recognition, Neurocomputing 365 (2019) 62–70.
[10] L. Yang, G. Yang, K. Wang, F. Hao, Y. Yin, Finger vein recognition via sparse reconstruction error constrained low-rank representation, IEEE Transactions on Information Forensics and Security 16 (2021) 4869–4881.
[11] X. Meng, J. Zheng, X. Xi, Q. Zhang, Y. Yin, Finger vein recognition based on zone-based minutia matching, Neurocomputing 423 (2021) 110–123.

[12] L. Yang, G. Yang, Y. Yin, X. Xi, Finger vein recognition with anatomy structure analysis, IEEE Transactions on Circuits and Systems for Video Technology 28 (8) (2018) 1892–1905.
[13] L. Yang, G. Yang, X. Xi, K. Su, Q. Chen, Y. Yin, Finger vein code: From indexing to matching, IEEE Transactions on Information Forensics and Security 14 (5) (2019) 1210–1223.
[14] B. Hou, R. Yan, Convolutional autoencoder model for finger-vein verification, IEEE Transactions on Instrumentation and Measurement 69 (5) (2019) 2067–2074.
[15] W. Yang, C. Hui, Z. Chen, J.-H. Xue, Q. Liao, FV-GAN: Finger vein representation using generative adversarial networks, IEEE Transactions on Information Forensics and Security 14 (9) (2019) 2512–2524.
[16] B. Hou, R. Yan, ArcVein: Arccosine center loss for finger vein verification, IEEE Transactions on Instrumentation and Measurement 70 (2021) 1–11.
[17] J. Wright, A. Y. Yang, A. Ganesh, S. S. Sastry, Y. Ma, Robust face recognition via sparse representation, IEEE Transactions on Pattern Analysis and Machine Intelligence 31 (2) (2009) 210–227.
[18] Z.-Q. Zhao, Y.-m. Cheung, H. Hu, X. Wu, Corrupted and occluded face recognition via cooperative sparse representation, Pattern Recognition 56 (2016) 77–87.
[19] Y. Xin, Z. Liu, H. Zhang, H. Zhang, Finger vein verification system based on sparse representation, Applied optics 51 (25) (2012) 6252–6258.
[20] S. Shazeeda, B. A. Rosdi, Finger vein recognition using mutual sparse representation classification, IET Biometrics 8 (1) (2018) 49–58.
[21] X. Mei, H. Ma, Finger vein recognition algorithm based on improved weighted sparse representation, in: 2019 International Conference on Information Technology and Computer Application (ITCA), IEEE, 2019, pp. 6–8.
[22] R. Basri, D. W. Jacobs, Lambertian reflectance and linear subspaces, IEEE Transactions on Pattern Analysis and Machine Intelligence 25 (2) (2003) 218–233.
[23] D. L. Donoho, Y. Tsaig, Fast solution of ℓ_1-norm minimization problems when the solution may be sparse, IEEE Transactions on Information Theory 54 (11) (2008) 4789–4812.
[24] D. L. Donoho, For most large underdetermined systems of linear equations the minimal ℓ_1-norm solution is also the sparsest solution, Communications on pure and applied mathematics 59 (6) (2006) 797–829.
[25] A. Wagner, J. Wright, A. Ganesh, Z. Zhou, H. Mobahi, Y. Ma, Toward a practical face recognition system: Robust alignment and illumination by sparse representation, IEEE Transactions on Pattern Analysis and Machine Intelligence 34 (2) (2012) 372–386.
[26] W. Deng, J. Hu, J. Guo, Extended SRC: Undersampled face recognition via intraclass variant dictionary, IEEE Transactions on Pattern Analysis and Machine Intelligence 34 (9) (2012) 1864–1870.
[27] Y. Xu, D. Zhang, J. Yang, J.-Y. Yang, A two-phase test sample sparse representation method for use with face recognition, IEEE Transactions on Circuits and Systems for Video Technology 21 (9) (2011) 1255–1262.
[28] W. Deng, J. Hu, J. Guo, In defense of sparsity based face recognition, in: IEEE/CVF Conference on Computer Vision and Pattern Recognition (CVPR), IEEE, 2013, pp. 399–406.
[29] D. Mery, K. Bowyer, Face recognition via adaptive sparse representations of random patches, in: Information Forensics and Security (WIFS), 2014 IEEE International Workshop on, IEEE, 2014, pp. 13–18.
[30] W. Yang, Q. Rao, Q. Liao, Personal identification for single sample using finger vein location and direction coding, in: Hand-Based Biometrics (ICHB), 2011 International Conference on, IEEE, 2011, pp. 1–6.
[31] M. Yang, L. Van Gool, L. Zhang, Sparse variation dictionary learning for face recognition with a single training sample per person, in: Proceedings of the IEEE international conference on computer vision, 2013, pp. 689–696.
[32] T.-H. Chan, K. Jia, S. Gao, J. Lu, Z. Zeng, Y. Ma, PCANet: A simple deep learning baseline for image classification?, IEEE transactions on image processing 24 (12) (2015) 5017–5032.
[33] L. Fei, B. Zhang, L. Zhang, W. Jia, J. Wen, J. Wu, Learning compact multifeature codes for palmprint recognition from a single training image per palm, IEEE Transactions on Multimedia 23 (2021) 2930–2942.
[34] L. Zhuang, T.-H. Chan, A. Y. Yang, S. S. Sastry, Y. Ma, Sparse illumination learning and transfer for single-sample face recognition with image corruption and misalignment, International Journal of Computer Vision 114 (2-3) (2015) 272–287.
[35] M. S. M. Asaari, S. A. Suandi, B. A. Rosdi, Fusion of band limited phase only correlation and width centroid contour distance for finger based biometrics, Expert Systems with Applications 41 (7) (2014) 3367–3382.
[36] Dataset: THU-FVFDT2 (2014). URL https://www.sigs.tsinghua.edu.cn/labs/vipl/thu-fvfdt.html
[37] Y. Tian, Y. Wang, D. Krishnan, J. B. Tenenbaum, P. Isola, Rethinking few-shot image classification: A good embedding is all you need?, in: European Conference on Computer Vision (ECCV), Springer International Publishing, 2020, pp. 266–282.
[38] Z. Sun, J. Wu, X. Li, W. Yang, J.-H. Xue, Amortized Bayesian prototype meta-learning: A new probabilistic meta-learning approach to few-shot image classification, in: International Conference on Artificial Intelligence and Statistics, PMLR, 2021, pp. 1414–1422.
[39] H. Li, D. Eigen, S. Dodge, M. Zeiler, X. Wang, Finding task-relevant features for few-shot learning by category traversal, in: IEEE/CVF Conference on Computer Vision and Pattern Recognition (CVPR), 2019, pp. 1–10.
[40] Z. Wang, L. Liu, Y. Duan, D. Tao, SIN: Semantic inference network for few-shot streaming label learning, IEEE Transactions on Neural Networks and Learning Systems (2022) 1–14.
[41] L. Fei-Fei, R. Fergus, P. Perona, One-shot learning of object categories, IEEE Transactions on Pattern Analysis and Machine Intelligence 28 (4) (2006) 594–611.
[42] H. Zhu, P. Koniusz, EASE: Unsupervised discriminant subspace learning for transductive few-shot learning, in: IEEE/CVF Conference on Computer Vision and Pattern Recognition (CVPR), 2022, pp. 9068–9078.
[43] X. Li, Z. Sun, J.-H. Xue, Z. Ma, A concise review of recent few-shot meta-learning methods, Neurocomputing 456 (2021) 463–468.
[44] Y. Yin, L. Liu, X. Sun, Sdumla-hmt: a multimodal biometric database, in: Chinese Conference on Biometric Recognition, Springer, 2011, pp. 260–268.
[45] A. Uhl, C. Busch, S. Marcel, R. Veldhuis, Handbook of vascular biometrics, Springer Nature, 2020.
[46] K. Wang, G. Chen, H. Chu, Finger vein recognition based on multi-receptive field bilinear convolutional neural network, IEEE Signal Processing Letters 28 (2021) 1590–1594.
[47] H. G. Hong, M. B. Lee, K. R. Park, Convolutional neural network-based finger-vein recognition using NIR image sensors, Sensors 17 (6) (2017) 1297–1319.
[48] Z. Fan, D. Zhang, X. Wang, Q. Zhu, Y. Wang, Virtual dictionary based kernel sparse representation for face recognition, Pattern Recognition 76 (2018) 1–13.
[49] W. Yang, W. Ji, J.-H. Xue, Y. Ren, Q. Liao, A hybrid finger identification pattern using polarized depth-weighted binary direction coding, Neurocomputing 325 (2019) 260–268.
[50] B. A. Rosdi, C. W. Shing, S. A. Suandi, Finger vein recognition using local line binary pattern, Sensors 11 (12) (2011) 11357–11371.
[51] D. Zhang, Z. Guo, G. Lu, L. Zhang, Y. Liu, W. Zuo, Online joint palmprint and palmvein verification, Expert Systems with Applications 38 (3) (2011) 2621–2631.
[52] W. Yang, X. Huang, F. Zhou, Q. Liao, Comparative competitive coding for personal identification by using finger vein and finger dorsal texture fusion, Information Sciences 268 (2014) 20–32.

Pengyang Zhao received the B.S. degree in information engineering from Jilin University in 2017. He is currently pursuing the Ph.D. degree with the Department of Electronic Engineering, Tsinghua University. His research interests include biometrics, pattern recognition and computer vision.

Zhiquan Chen received the B.S. degree in communication engineering from Jilin University in 2015, and the M.S. degree from the Department of Electronic Engineering, Tsinghua University, in 2018. His research interests include biometrics and finger vein recognition.

Jing-Hao Xue received the Dr.Eng. degree in signal and information processing from Tsinghua University in 1998 and the Ph.D. degree in statistics from the University of Glasgow in 2008. He is a Professor of Statistical Pattern Recognition in the Department of Statistical Science, University College London. His research interests include statistical pattern recognition, machine learning and computer vision. He is an Associate Editor of IEEE Transactions on Circuits and Systems for Video Technology, IEEE Transactions on Cybernetics, and IEEE Transactions on Neural Networks and Learning Systems.

Jianjiang Feng received the B.Eng. and Ph.D. degrees from the School of Telecommunication Engineering, Beijing University of Posts and Telecommunications, China, in 2000 and 2007, respectively. From 2008 to 2009, he was a Post-Doctoral Researcher with the PRIP Laboratory, Michigan State University. He is currently an Associate Professor with the Department of Automation, Tsinghua University, Beijing. His research interests include fingerprint recognition and computer vision. He is an Associate Editor of the Image and Vision Computing.

Wenming Yang received his Ph.D. degree in information and communication engineering from Zhejiang University in 2006. He is an Associate Professor in Shenzhen International Graduate School / Department of Electronic Engineering, Tsinghua University. His research interests include image processing, pattern recognition, computer vision and AI in medicine.

Qingmin Liao received the Ph.D. degree in signal processing and telecommunications from the University of Rennes 1 in 1994. He is currently a Professor in Shenzhen International Graduate School / Department of Electronic Engineering, Tsinghua University. His research interests include image/video processing, transmission, analysis, biometrics, and their applications.

Jie Zhou received the B.S. and M.S. degrees from the Department of Mathematics, Nankai University, Tianjin, China, in 1990 and 1992, respectively, and the Ph.D. degree from the Institute of Pattern Recognition and Artificial Intelligence, Huazhong University of Science and Technology, Wuhan, China, in 1995. From 1995 to 1997, he served as a Post-Doctoral Fellow with the Department of Automation, Tsinghua University, Beijing, China. Since 2003, he has been a Full Professor with the Department of Automation, Tsinghua University. His current research interests include computer vision, pattern recognition, and image processing.